Erosive versus shadowing instabilities in the self-organized ion patterning of polycrystalline metal films

A. Toma,[1] D. Chiappe,[1] B. Šetina Batič,[2] M. Godec,[2] M. Jenko,[2] and F. Buatier de Mongeot[1,*]
[1]*CNISM and Dipartimento di Fisica, Università di Genova, via Dodecaneso 33, 16146 Genova, Italy*
[2]*Inštitut za kovinske materiale in tehnologije, Lepi pot 11, 1000 Ljubljana, Slovenia*
(Received 26 August 2008; published 21 October 2008)

We report on the self-organized patterning of polycrystalline metal films supported on dielectric substrates using defocused Ar^+ ion-beam sputtering at glancing incidence. The data demonstrate that a nonflat initial surface morphology does plays a critical role in triggering self-organization during the early stages, where the distribution of polycrystalline grains initially imposes a nonstochastic spatial modulation of the ion impact sites. A crossover to the conventional erosive regime observed for single crystals sets in at longer sputtering times. Surprisingly, the vertical and lateral modulation of the pristine surface profile of the nonflat films results in a substantial reduction in the ion dose required for the formation of the nanoscale patterns, in comparison to the case of an initially flat film.

DOI: 10.1103/PhysRevB.78.153406 PACS number(s): 81.16.Rf, 61.80.Jh, 68.65.−k

Self-organized physical approaches are actively investigated as a viable alternative to top-down methods for nanoscale pattern formation over macroscopic areas. Periodic patterns (mound or ripplelike) have been observed on substrates subject to defocused ion-beam sputtering (IBS).[1–4] According to the Bradley-Harper (BH) theory,[5] pattern formation originates from a curvature-dependent sputtering yield which promotes faster erosion of the valleys in comparison to the crests, and wavelength selection results from a competition between diffusive relaxation and ion-induced erosive instability.

A general basic assumption common to the theoretical models employed for describing pattern formation during ion irradiation is to consider the starting morphology as a flat surface profile, subject to a temporally and spatially stochastic roughening term, due to the random arrival of ions. This leads to a slow evolution of the surface modulation (roughness and wavelength) which, in the case of metal substrates, generally follows a power-law behavior.[1,6–8] Though the linear version of the BH model does not predict coarsening of the metal nanostructures produced by IBS, it provides a useful handle for describing the essential features of the process.[1,2] From a fundamental as well as from an applied point of view, it is of interest to understand in which way the morphological evolution is modified by a nonflat initial topography which presents vertical and lateral modulations comparable to the typical periodicity of the nanostructures. This is the situation usually met in polycrystalline metal films with a characteristic grain distribution which depends on the growth procedure.[9–12]

An additional question has to be addressed for describing pattern formation in polycrystalline films. Here mass transport of mobile species (adatom and vacancy diffusion) can be affected by the presence of submicron grains with different in-plane orientations: in the polycrystalline case in fact, an upper limit for diffusion could be set by the grain boundaries, while the random in-plane grain orientation is acting as a *local* source for diffusion anisotropy.[9–14]

We provide evidence that, at the early stages of glancing angle irradiation of nonflat substrates, the vertical and lateral grain distribution spatially modulates the flux of impinging ions in a nonstochastic way (through a shadowing instability) thus promoting the growth of ripples with an initial lateral periodicity imposed by the dominant primitive features. For increasing ion doses a crossover to the trend observed on single crystalline metal substrates is found. Surprisingly, in the case of the nonflat films, the kinetics of pattern formation receives a *head start* from the initial roughness distribution, resulting in a reduction in the ion dose required for the formation of the nanoscale patterns, in comparison to the case of initially flat films. Additionally, we demonstrate that the presence of grain boundaries does not impede the coherent propagation of ripples which elongate over several micrometers. Some recent preliminary attempts have appeared, which demonstrated ripple formation on polycrystalline films subject to IBS; however, the issues of grain-size distribution and of the initial roughness profile of the films were overlooked.[15–17]

We investigated the evolution of the nanoscale pattern employing *ex situ* atomic force microscopy (AFM) and scanning electron microscopy (SEM), with the aim of correlating the initial surface morphology with the successive pattern evolution. For this purpose, we studied polycrystalline Au films grown adopting different deposition procedures (but with the same starting thickness—150 nm) which result in a broad range of grain sizes and roughness distribution.[9–14] In agreement with Refs. 9 and 10 the Au films present a (111) texture as revealed by x-ray diffraction (XRD) measurements (data not shown).

In Fig. 1 we show SEM investigations of the flat Au films acquired in backscattered electron imaging (BEI) mode. The films grown by sputter deposition [Fig. 1(a)] present the narrower distribution of grain sizes with a significant fraction of the grains with a diameter around 70 nm and a smaller population of grains with diameters around 100 nm (the surface roughness obtained by additional AFM images is about 4 nm).

For the films grown by thermal evaporation [Fig. 1(b)] the population of smaller grains around 80 nm is still abundant, but a significant fraction of the grains coarsens into bigger

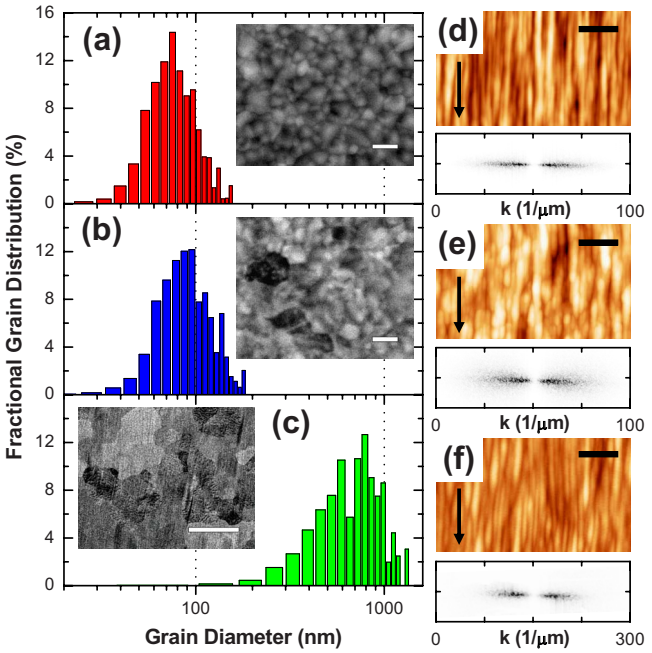

FIG. 1. (Color online) Grain-size distribution (fractional surface coverage) of the Au films obtained from SEM imaging. The 150-nm-thick films were grown by different procedures: (a) sputter deposition, (b) thermal evaporation, (c) flame annealing. The SEM scale bars are, respectively, 100 nm, 100 nm, and 1 μm. (d)–(f) AFM images of the Au films in (a)–(c) after ion irradiation at the same dose 7×10^{17} ions/cm^2. Insets: 2D-FFT of the AFM images. The AFM scale bars are 600 nm for (d), (e) and 200 nm for (f).

ones with diameters around 130 nm possibly due to the lower deposition flux of 6 nm/min compared to the sputter deposited films (rate 18 nm/min). In the same way also the initial roughness is increased up to $\sim$6 nm. If very smooth films with grain sizes exceeding the micrometer range are looked for, one possibility is to use flame annealed Au films deposited on freshly cleaved mica substrates.[18] In that case [Fig. 1(c)], the initial roughness is reduced to 1 nm and a very broad distribution of (111) terminated grains centered around 800 nm is formed, with a significant fraction of the grain diameters exceeding 1 μm.

The polycrystalline Au samples have been exposed to defocused ion-beam irradiation from a gridded multiaperture Ar^+ source. We chose a grazing sputtering angle $\theta=82°$ and a sputtering energy $E=800$ eV, while the ion dose was varied in the range between $\Theta=2.3\times10^{17}$ ions/cm^2 and 2.2×10^{18} ions/cm^2 at a constant flux of 5.5×10^{14} ions/cm^2 sec (measured in a plane parallel to the sample surface). The sample holder temperature was controlled around $T\sim230$ K during the sputtering process (by means of a liquid nitrogen cooling system) in order to prevent excessive ion-induced surface heating. Under such conditions the surface temperature (as determined by means of an infrared pyrometer) was stabilized around $T\sim300$ K.

Figures 1(d)–1(f) show representative AFM images of the different Au surfaces irradiated with the same ion dose of 7×10^{17} ions/cm^2. The ripples are elongated parallel to the projection of the ion beam. Measurements of the average ripple wavelength Λ derived from the two-dimensional (2D) fast Fourier transform (FFT) of the AFM images, after differential filtering in order to enhance the ripple contrast [insets of Figs. 1(d)–1(f)], show that after ion irradiation a well-defined elongation in the beam direction is visible and the estimated value of the ripple periodicity can vary from $\Lambda=(70\pm3)$ nm to $\Lambda=(120\pm10)$ nm for the samples prepared by sputter and thermal deposition, respectively. These periodicities are in quantitative agreement with the lateral size distribution of the dominant grains in the pristine samples described in Figs. 1(a) and 1(b).

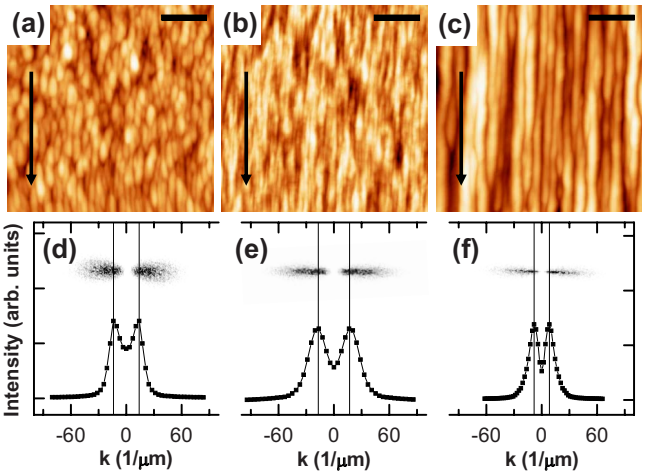

FIG. 2. (Color online) Representative AFM morphologies (scale bar=600 nm) of the Au films grown by sputter deposition and irradiated with Ar^+ at increasing fluences Θ: (a) 2.3×10^{17} ions/cm^2, (b) 5×10^{17} ions/cm^2, (c) 2.2×10^{18} ions/cm^2. The corresponding 2D-FFT with line cut along the ripple wave vector is shown below.

The situation is completely modified if we attempt to pattern the film of Fig. 1(c) which has grain sizes well exceeding the typical ripple wavelengths. In this case each of the grains locally behaves as a flat monocrystalline Au(111) surface: the dynamics of the rippling instability is foreseen to be similar to the single-crystal (SC) case (in the following called SC erosive regime) as described by the BH model for grazing incidence conditions.[1,2] The nonequivalence of the nanoscale pattern formation on films with nonflat initial morphology, after irradiation to the same dose [Figs. 1(d)–1(f)], provides a clear indication that under glancing angle irradiation conditions, the nonstochastic spatial modulation of ion impact sites imposed by the vertical grain distribution is playing a key role.

In order to better clarify this issue, the evolution of surface morphology was studied as a function of ion fluence, from $\Theta=2.3\times10^{17}$ ions/cm^2 to 2.2×10^{18} ions/cm^2, for the films of Fig. 1. In Fig. 2 we present a time sequence of the morphology of the Au films grown by sputter deposition. After an irradiation dose as short as 2.3×10^{17} ions/cm^2, the distribution of grains [Fig. 2(a)] appears slightly elongated along the beam projection (arrow). One important aspect to point out is the lateral size of the incipient ripples: it is in the 70 nm range, similar to the grain-size distribution of the pristine film. For increasing dose, the elongation of the ridges becomes well pronounced [Fig. 2(b)]. Remarkable ripple elongations, which can be comparable to the AFM

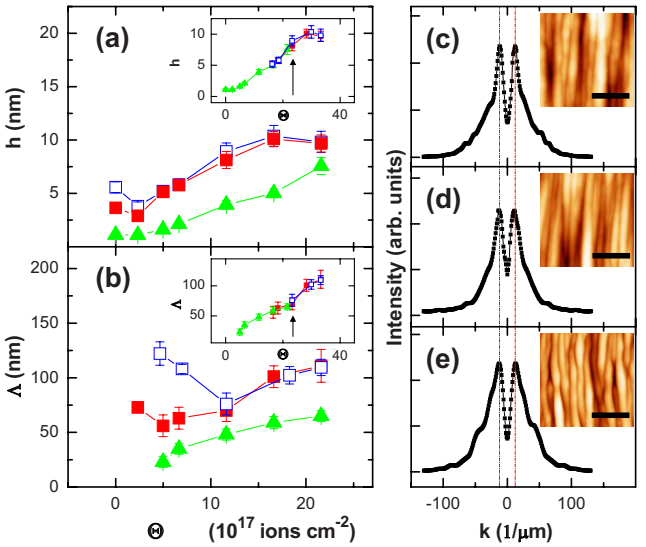

FIG. 3. (Color online) (a) Average amplitude h and (b) periodicity Λ of the nanostructures vs ion fluence Θ derived from the AFM images. Red filled squares and panel (c) refer to sputter deposited, blue open squares and (d) to thermal evaporated, green filled triangles and (e) to flame annealed Au films. Inset: horizontal rigid shift ($\Delta\Theta = 1.2 \times 10^{18}$ ions/cm^2) of the curves representing the rough samples (open, filled squares). (c)–(e) Topographs (with the same vertical range=35 nm) of the different sample series irradiated with identical *scaled* ion doses. The respective 2D-FFT line cuts evidence the equivalence of Λ.

image size (3 μm), and well exceeding the average grain size, are found increasing the ion dose up to 2.2×10^{18} ions/cm^2 [Fig. 2(c)].

These observations are quantitatively summarized in Fig. 3, where the result of a statistical analysis on a significant number of AFM images has been reported. Here we plot the ripple periodicity (wavelength Λ) derived from the peak position in the FFT profile and the ripple amplitude h defined as the average peak to valley excursion in the one-dimensional (1D)-AFM line scan (neglecting the large scale lateral modulations). In the case of the flat film (filled triangles) a monotonic steady increase in the ripple amplitude [Fig. 3(a)] and wavelength [Fig. 3(b)] is found. According to the BH theory, the ion-driven buildup of surface roughness is stochastic and comparatively large doses are needed before a well-defined corrugation evolves. The minimum wavelength which can be observed by AFM, on the order of 20 nm, is compatible with the results observed in the case of single-crystal metal surfaces.[1,19] The situation is markedly different in the case of the initially nonflat Au films (filled and open squares). With increasing dose we can notice two things: (i) the initial selection of a Λ closely related to the dominant grain sizes in the polycrystalline films, and a *decrease* in the dominant ripple wavelength until a threshold dose is reached (for the sputter deposited film—full squares in Fig. 3—around $\Theta = 5 \times 10^{17}$ ions/cm^2); (ii) the subsequent monotonic increase in Λ at higher fluences, which is in agreement with the trend observed for the single-crystal surfaces[1] and for the flat flame annealed Au samples (filled triangles in Fig. 3). The thermally evaporated Au films (open squares) present a very

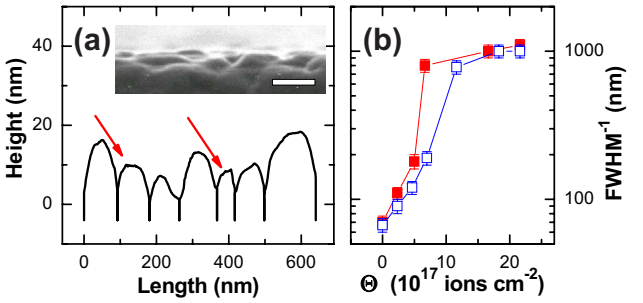

FIG. 4. (Color online) (a) AFM line profile of the Au films grown by thermal evaporation (vertical scale amplified). A representative SEM micrograph is shown in the inset (scale bar 100 nm). (b) Evolution with fluence of the FWHM^{-1} data derived from cuts of the 2D-FFT peak along the ripple in-channel direction. Red filled squares refer to sputter deposited, blue open squares to thermal evaporated Au films.

similar decreasing behavior, but in this case the transition dose is shifted at about 1.2×10^{18} ions/cm^2, due to the initially larger roughness and grain size.

Our interpretation is based on the observation that under the very grazing ion incidence conditions employed here, the lateral distribution of the ion impact sites becomes nonstochastic and spatially modulated by the local surface corrugation of the pristine grain distribution. We can visualize this with the aid of the SEM micrograph in the inset of Fig. 4(a), representing a cross section of a polycrystalline Au film (grown by thermal deposition). In panel (a) a representative AFM line profile is shown (red arrows indicate the ion-beam incidence angle, $\theta \sim 82°$, according to the vertical scale expansion). Regions behind large and tall grains are shadowed from the ion beam and thus experience a reduced erosion rate, while regions behind small and shallow grains or in the valleys are eroded efficiently, resulting in a self-leveling mechanism of the ripple ridges along the ion-beam projection. The initial wavelength selection is thus driven by a *shadowing instability* in which the taller (and larger) grains select a ripple wavelength that is different from the value expected for a flat film, at comparable ion fluences, in a pure SC erosive regime [Fig. 3(b), filled triangles]. For increasing dose, when the differences in height of adjacent grains level off along the beam projection, the lateral distribution of impact sites becomes progressively stochastic, and the shadowing instability is surpassed by the conventional SC erosive instability. The reciprocal of the full width at half maximum (FWHM^{-1}) of the FFT peak along the ripple in-channel direction (black lines in Fig. 2) provides a sensitive estimate of the average ripple elongation and quantitatively evidences the steady evolution of the self-leveling process [Fig. 4(b)]. We find a saturation of the FWHM^{-1} (ripple elongation comparable to the AFM image size) for doses exceeding 1.2×10^{18} ions/cm^2 for the Au thermally evaporated samples, and at 5×10^{17} ions/cm^2 for the sputter deposited ones, in correspondence to the crossover to the SC erosive regime.

The decreasing trend of Λ could be qualitatively understood with the aid of the BH linear model which predicts the existence of an *intrinsic* wave mode (Λ^*) growing faster than all the other ones. The amplification rate given by the BH

dispersion relation is positive at all long wavelengths, peaked at Λ^* and negative for some critical wavelength below Λ^*.[20] As shown in Fig. 3, the intrinsic BH wavelength, Λ^*, found for single-crystal-like films (filled triangles) is well below the initial wavelength imposed by the shadowing instability (full and open squares) even taking into account the slow increase in Λ due to coarsening. For increasing ion doses we can thus expect that the BH wave modes around Λ^* will be amplified more, shifting downward the initial wavelength distribution of the nonflat films.

A further important result can be derived from the data in Figs. 3(a) and 3(b) (filled squares, empty squares): the initial grain-size distribution of the nonflat films (open and filled squares) is responsible for a significant reduction in the ion dose required for the formation of the ripples in comparison to the case of a flat surface (filled triangles). In the latter case, ripples of comparable Λ and h are formed only after a substantially larger irradiation dose. In the insets of Figs. 3(a) and 3(b) we can easily recognize that a horizontal rigid shift of the data relative to the nonflat films (open and filled squares) by $\Delta\Theta = +1.2 \times 10^{18}$ ions/cm^2 leads to a collapse of the data points (both of Λ and of h) over the SC erosive curve (filled triangles). Sample topographies of the different series, irradiated with identical *scaled* ion doses of 2.2×10^{18} ions/cm^2, are shown in Figs. 3(c)–3(e). The respective two-dimensional fast Fourier transform (2D-FFT) line cuts evidence the equivalence of the ripple periodicity. This implies that, for an initial topography possessing wave modes that are amplified within the BH linear model, the subsequent evolution is receiving a head start with respect to the flat initial case.[20] The primitive roughness of the polycrystalline film can thus efficiently reduce the ion dose required for the formation of ripple modulations on a flat film, without however changing the dynamic evolution of the ripples at the later stages [the scaling of Λ and h versus dose Θ is equivalent for the flat and nonflat films; see insets of Figs. 3(a) and 3(b)].

These results, corroborated by further SEM images (data not shown), underline the role of the *topographic* roughness in determining pattern formation. Though the presence of submicron grains with different in-plane orientations might hinder intergrain diffusion of mobile particles, for glancing ion sputtering conditions employed here, the ripple orientation is imposed by the beam projection (SC erosive regime) and coherent ripple propagation is observed across several microns. On the more applied side, the present observations support the extension of the results derived from single crystals to the technologically relevant class of polycrystalline films, and suggest the use of substrates with an artificially corrugated morphology for triggering, via a shadowing instability, the formation of a pattern with a periodicity imposed by the primitive features.[21]

In summary, we used SEM and AFM to observe the surface nanostructuring of metal films with a controlled nonflat starting morphology exposed to ion-beam sputtering at grazing incidence angles. We correlated the initial changes in surface morphology with the topographic modulations imposed by the pristine grain distribution, demonstrating that a nonflat initial morphology can play a critical role in triggering self-organization via a shadowing instability. A crossover to the conventional erosive regime observed for single crystals sets in at longer sputtering times. Remarkably a substantial reduction in the ion dose required for the formation of the ripples is observed for the nonflat films in comparison to the flat case.

Useful discussions with U. Valbusa and C. Boragno are acknowledged. This work was supported by CNISM (fondi CNR-INFM progetto INNESCO), and in part by MAE under programs Italia-Slovenia and Italia-Polonia and by Fondazione CARIGE (A.T.).

*Corresponding author; buatier@fisica.unige.it

[1] U. Valbusa, C. Boragno, and F. Buatier de Mongeot, J. Phys.: Condens. Matter **14**, 8153 (2002).
[2] W. L. Chan and E. Chason, J. Appl. Phys. **101**, 121301 (2007).
[3] G. Costantini, F. Buatier de Mongeot, C. Boragno, and U. Valbusa, Phys. Rev. Lett. **86**, 838 (2001).
[4] S. Facsko, T. Dekorsy, C. Koerdt, C. Trappe, H. Kurz, A. Vogt, and H. L. Hartnagel, Science **285**, 1551 (1999).
[5] R. M. Bradley and J. M. Harper, J. Vac. Sci. Technol. A **6**, 2390 (1988).
[6] S. van Dijken, D. de Bruin, and B. Poelsema, Phys. Rev. Lett. **86**, 4608 (2001).
[7] A. Redinger, H. Hansen, U. Linke, Y. Rosandi, H. M. Urbassek, and T. Michely, Phys. Rev. Lett. **96**, 106103 (2006).
[8] A. Molle, F. Buatier de Mongeot, A. Molinari, C. Boragno, and U. Valbusa, Phys. Rev. B **73**, 155418 (2006).
[9] C. V. Thompson, Annu. Rev. Mater. Sci. **30**, 159 (2000).
[10] M. J. Rost, D. A. Quist, and J. W. M. Frenken, Phys. Rev. Lett. **91**, 026101 (2003).
[11] C. Polop, C. Rosiepen, S. Bleikamp, R. Drese, J. Mayer, A. Dimyati, and T. Michely, New J. Phys. **9**, 74 (2007).
[12] M. J. Rost, Phys. Rev. Lett. **99**, 266101 (2007).
[13] C. W. Pao, S. M. Foiles, E. B. Webb, D. J. Srolovitz, and J. A. Floro, Phys. Rev. Lett. **99**, 036102 (2007).
[14] J. S. Tello, A. F. Bower, E. Chason, and B. W. Sheldon, Phys. Rev. Lett. **98**, 216104 (2007).
[15] P. Karmakar and D. Ghose, Surf. Sci. **554**, L101 (2004).
[16] K. Zhang, F. Rotter, M. Uhrmacher, C. Ronning, J. Krauser, and H. Hofsäss, New J. Phys. **9**, 29 (2007).
[17] M. Stepanova and S. K. Dew, J. Vac. Sci. Technol. B **24**, 592 (2006).
[18] C. Nogues and M. Wanunu, Surf. Sci. **573**, L383 (2004).
[19] G. Bracco and D. Cavanna, Phys. Rev. B **76**, 033411 (2007).
[20] B. Davidovitch, M. J. Aziz, and M. P. Brenner, Phys. Rev. B **76**, 205420 (2007).
[21] A. Cuenat, H. B. George, K. C. Chang, J. M. Blakely, and M. J. Aziz, Adv. Mater. (Weinheim, Ger.) **17**, 2845 (2005).